Indian Journal of Pure & Applied Physics
Vol. 58, December 2020, pp. 892-908

MHD variable viscosity mixed convection of nanofluid in a microchannel with permeable walls

Mesfin Zewde Kefene[a]*, Oluwole Daniel Makinde[b] & Lemi Guta Enyadene[c]

[a]Department of Applied Mathematics, Adama Science and Technology University, Adama, Ethiopia

[b]Faculty of Military Science, Stellenbosch University, Private Bag X2, Saldanha 7395, South Africa

[c]Department of Applied Mathematics, Adama Science and Technology University, Adama, Ethiopia

Received 15 June 2020; accepted 8 October 2020

In this study, we examine the combined effects of buoyancy forces, pressure gradient, thermophoresis, Brownian motion, variable viscosity of nanofluid flow in a microchannel with suction and injection in the presence of uniform magnetic field imposed in cross-wise direction. It is assumed that the dynamic viscosity of the nanofluid is related with temperature exponentially and that the vertical parallel-plates temperature is held asymmetrically. Applying similarity transformation, the governing system of partial differential equations (PDEs) are transformed into a set of non-dimensional nonlinear partial differential equations whose solutions are obtained numerically by semi-discretization centered finite difference method along with *Runge-Kutta Fehlberg* integration technique scheme. Qualitative description of graphical results depicting the effect of thermophysical parameters on the dimensionless velocity, temperature, nanoparticles concentration, skin friction, Nusselt number and Sherwood number are presented.

Keywords: MHD; nanofluid; permeable microchannel; Mixed convection; Variable viscosity; Suction/injection; Buongiorno model.

1 Introduction

The modern advancement of High-Tech industries equipments such as electronic computers, x-rays and car engines have been associated with continuous miniaturization of the size of components and augmentation in their power and heat generation. Useful heat removal strategies are, therefore, required to keep the safe and efficient operations of these components. Adopting microchannels in the components, it endowed with high heat removal capacity and reduced temperature gradient from components[1-4]. These properties of microchannels make them applicable in the cooling of High-Tech industries equipments. Moreover, microchannels have interesting applications in drug delivery for medicine, cooling for microelectronic[5] and pumping technology for medical enginering[6]. The above practical applications arouse the interest of researchers to investigate fluid flow and heat transfer in microchannels[7-13]. Kandlikar *et al.*[14] exhaustively studied fluid flow and heat transfer in minichannels and microchannels. They analyzed single phase flow of gas, liquid and electronics in microchannels. Also, they have seen boiling, condensation and biomedical application aspects of microchannel flow. Markal *et al.*[15] investigated experimentally deionized water laminar flow through microchannel heat sinks (MCHS). The MCHS has twenty nine parallel rectangular channel, and three channel geometries with aspect ratio (1.2, 0.82 and 0.37). They considered the Reynolds number ranges from 12.3 to 47.3 and found that increasing aspect ratio increases Nusselt number and decreasing the friction factor.

The flow of electrically conducting fluid through a microchannel in the presence of applied magnetic field transversely has many applications in magneto-hydrodynamic (MHD) power generator, cooling of micro-nuclear reactor, MHD micro-pump. In the recent past years, MHD fluid flow in microchannel were studied by Jha *et al.*[16,17], Das *et al.*[18], Malvind and Ganji[19], Shashikumar *et al.*[20], and Aina and Malgwi[21]. Jha *et al.*[16] investigated the effect of transverse-wise imposed magnetic field on steady natural convection flow of conducting fluid in a microchannel. Their results show that an increase in Hartmann number, decreases the volume flow rate, skin friction at the left wall, and increases at right wall. Jha *et al.*[17] studied transient fully developed natural convection flow of electrically conducting

*Corresponding author: (E-mail: mesfink2005@gmail.com)

fluid in vertical micro-concentric-annuli under the influence of transverse direction applied magnetic field. It is found that an increase in Hartmann number yields decreasing the fluid velocity, the volume flow rate, skin friction and an increase in velocity slip at the surface of the cylinder. Das *et al.*[18] discussed fully developed mixed convection flow in a vertical channel filled with nanofluids in the presence of a uniform transverse magnetic field. The effects of prominent parameters on nanofluid velocity, temperature and induced magnetic field as well as the shear stress and the rate of heat transfer at the channel wall are qualitatively analyzed. Malvind and Ganji[19] analysed the combined effects of nanoparticle parameter, buoyancy force and Hartmann number on nanofluid flow and heat transfer through microchannel. They found that the velocity profile, the dimensionless heat transfer coefficient decrease with an increased Hartmann number. Shashikumar *et al.*[20] investigated numerically the heat transfer and entropy generation of MHD casson fluid flow through a permeable microchannel in the presence of thermal radiation. Their results indicate that the velocity profile of the fluid decreases with increasing Hartmann number and both suction/injection parameter. Aina and Malgwi[21] examined the effect of transverse magnetic field and suction/injection on natural convection conducting fluid flow in an inclined permeable microchannel. Their outcomes entail that the fluid velocity dwindled with increasing Hartmann number and injection where as decreased with increasing inclination angle and suction.

Nanofluids are engineered suspensions consist of nanoparticles dispersed in a base fluid. In the world of advanced technology, microfluidics and nanotechnology, the flow of nanofluid in microchannels has a significant role in applications such as cooling of microchips, cancer theraupetics, nanocryosurgery and nanodelivery[22-24]. The problem of microchannel flow using nanofluids has been investigated by several researchers including[25-28]. Malvind and Ganji[29] studied theoretically fully developed mixed convection flow of alumina/water nanofluid and heat transfer in a vertical microchannel in the presence of heat source/sink with asymmetric wall heat fluxes. Belhadj *et al.*[30] analyzed numerically the heat transfer performance of MCHS filled with fully developed laminar forced convection flow of water/Al_2O_3 nanofluid. They found that Nusselt number increases with increasing Reynolds number and nanoparticle concentration. Snoussi *et al.*[31] studied numerically a laminar nanofluid flow and heat transfer in a 3D MCHS with a constant heat flux by FLUENT software. They obtained that increasing the heat flux shows the heat transfer coefficient of MCHS strongly intensified in the presence of nanofluid and not affected with pure water. Pordanjani *et al.*[32] numerically investigated the effects of magnetic field, joule heating, Brinkman number, Reynolds number, and nanofluid concentration on laminar forced convection flow of water-Al_2O_3 nanofluid in a parallel plate microchannel by a control volume finite different scheme. Their results imply that Hartmann number, Joule number, Brinkman number, Reynolds number, and nanofluid concentration have a reduction effect on the heat transfer from the wall. Nguyen *et al.*[33] studied the effects of applied magnetic field on heat transfer and entropy generation of nanofluid flow through microchannel with a corrugated wall. By considering slip velocity, they also analyzed the impacts of Reynolds and Hartmann number on Nusselt and Bejan numbers. Their results affirm that both slip velocity and magnetic field enhance the heat transfer and the entropy generation.

From suction and injection view point of fluid flow through microchannel with permeable walls, Jha *et al.*[34-36] studied the effect of suction/injection parameter and explained the behavior of velocity, temperature, skin friction and heat transfer in a microchannels. They identified that velocity, temperature, skin friction and heat transfers are dependent on suction/injection parameter.

In almost the literature reviewed above, fluid properties are assumed to be constant. Experimental results show that constant fluid properties remain valid only if rapid fluid temperature variation does not occur in the flow field. In a microchannel fluid flow, due to its smaller diameter there is a rapid change of kinetic energy of the flow to internal energy and this is resulting in high frictional resistance of the fluid/coolant in a microchannels and it leads to high temperature rise within the fluid flowing in the microchannel. So, fluid flow through microchannel has a significant effect on fluid properties of the coolant like viscosity, thermal conductivity because of the temperature rise in the flowing fluid. The most responsive fluid property to rapid temperature rise of fluid is viscosity[37]. Many engineering applications such as MHD microchannel generator, microreactor, microchannel heat exchanger, *etc.* are areas where

swift temperature change happens. In this way, many researchers have considered the influence of temperature dependent viscosity on heat transfer characteristics of nanofluid flow in a microchannel. Among which Khamis *et al.*[38] reported the effect of variable viscosity laminar unsteady nanofluid flow through permeable wall pipe with convective cooling. Prasad *et al.*[39] analysed the effects of variable transport properties with temperature on MHD mixed convection flow and heat transfer in a vertical channel. The combined effects of nonlinear thermal radiation, buoyancy force, convective cooling and viscous dissipation on inherent irreversibility and thermal stability of temperature dependent variable viscosity EG/Ag nanofluid flow in microchannels were studied by Monaledi and Makinde[40]. Makinde[41] has discussed the effect of temperature dependent viscosity in the study of variable viscosity EG/Ag nanofluids and heat transfer in microchannel with convective cooling. He found that increasing the viscosity parameter enhances the velocity, temperature and Nusselt number of the EG-water/Ag nanofluid. In the present study, our main objective is to investigate the simultaneous impact of buoyancy force, pressure gradient, thermophoresis, Brownian motion, magnetic field, variable viscosity on mixed convection flow of conducting fluid through vertical parallel plate microchannel with permeable walls.

2 Mathematical Formulations

We consider unsteady flow of an incompressible, temperature dependent variable viscosity MHD nanofluid in a vertical parallel-plate microchannel of width a units with permeable walls, where the left wall is kept at temperature of T_o and the right wall at T_1 such that $T_o < T_1$. A uniform transverse magnetic field B_o is applied in the direction parallel to $\bar{y}$ -axis. The schematic diagram is depicted in Fig. 1. It is assumed that a 2D-coordinate system is used, wherein the left wall is fixed at $\bar{x} = 0$, the right wall is fixed at $\bar{x} = a$ (the $\bar{x}$-axis is aligned vertically) and the $\bar{y}$ -axis is perpendicular to the wall.

The nanofluid flow within the microchannel is induced due to the combined effect of pressure gradient and the effect of buoyancy force. It is also considered that the magnetic Reynolds number is so meager that the induced magnetic field is ignored as compared to the imposed magnetic field. Using *Buongiorno* nanofluid flow model, MHD model equation and the usual *Oberbeck-Bousssinesq* approximation, the governing equations for continuity, momentum, energy and concentration are gven as:

$$\frac{\partial \bar{u}}{\partial \bar{x}} = 0, \qquad \ldots (1)$$

$$\frac{\partial \bar{u}}{\partial \bar{t}} + V\frac{\partial \bar{u}}{\partial \bar{y}} = -\frac{1}{\rho}\frac{\partial \bar{P}}{\partial \bar{x}} + \frac{1}{\rho}\left[\mu(T)\frac{\partial \bar{u}}{\partial \bar{y}}\right] - \frac{\sigma}{\rho}B_o^2\bar{u} + \beta_1 g(T - T_o) + \beta_2 g(C - C_o), \qquad \ldots (2)$$

$$\frac{\partial T}{\partial \bar{t}} + V\frac{\partial T}{\partial \bar{y}} = \alpha\frac{\partial^2 T}{\partial \bar{y}^2} + \tau\left[D_B\frac{\partial C}{\partial \bar{y}}\frac{\partial T}{\partial \bar{y}} + \frac{D_T}{T_o}\left(\frac{\partial T}{\partial \bar{y}}\right)^2\right] - \frac{\mu(T)}{\rho c_p}\left(\frac{\partial \bar{u}}{\partial \bar{y}}\right)^2 + \frac{\sigma B_o^2}{\rho c_p}\bar{u}, \qquad \ldots (3)$$

$$\frac{\partial C}{\partial \bar{t}} + V\frac{\partial C}{\partial \bar{y}} = D_B\frac{\partial^2 C}{\partial \bar{y}^2} + \frac{D_T}{T_o}\frac{\partial^2 T}{\partial \bar{y}^2}, \qquad \ldots (4)$$

with initial and boundary conditions:

$$\bar{u}(\bar{y},0) = 0, T(\bar{y},0) = T_o, C(\bar{y},0) = C_o, \qquad \ldots (5)$$

$$\bar{u}(0,\bar{t}) = 0, T(0,\bar{t}) = T_o, D_B\frac{\partial C}{\partial \bar{y}}(0,\bar{t}) = -\frac{D_T}{T_o}\frac{\partial T}{\partial \bar{y}}(0,\bar{t}), \quad \bar{u}(a,\bar{t}) = 0, T(a,\bar{t}) = T_1, C(a,\bar{t}) = C_1, \qquad \ldots (6)$$

where $\bar{u}$ is the nanofluid velocity in $\bar{x}$ -direction, T is the temperature of nanofluid, C is the nanoparticles concentration, V is the suction/injection velocity,

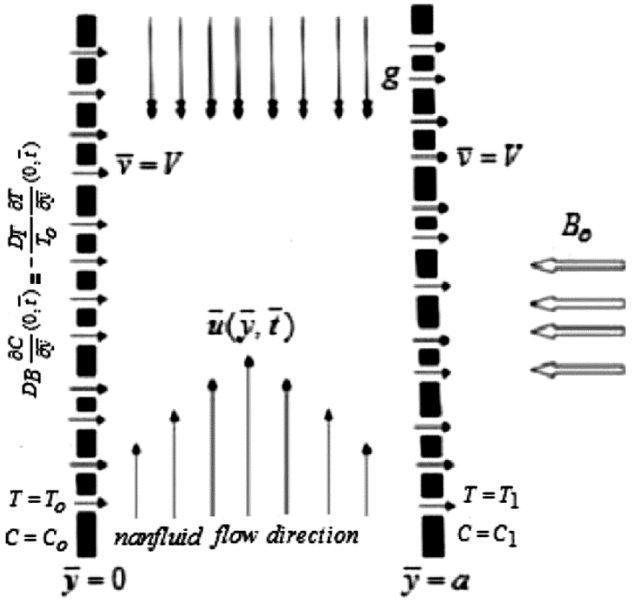

Fig. 1 — Flow geometry with coordinate system

P is the nanofluid pressure, $\bar{t}$ is the time, ρ is the density of nanofluid, μ is the viscosity of the nanofluid, g is the acceleration due to gravity, β_1 and β_2 are the thermal and solutal expansion coefficients respectively, α is the thermal diffusion coefficient, τ is the ratio between the effective heat capacity of nanoparticle material and heat capacity of the fluid, D_T is the thermophoretic diffusion coefficient, T_o is the temperature of the left wall, T_1 is the temperature of the right wall, σ is the electrical conductivity, a is the channel width, c_p is the specific heat at constant pressure. Using Makinde[42], the dynamic viscosity of the nanofluid is considered to be related with temperature exponentially such that

$$\mu(T) = \mu_o e^{-\gamma(T-T_o)}. \quad \ldots (7)$$

The above Eqs. 2-6 become non-dimensional form by using and incorporating the following variables and parameters:

$$x = \frac{\bar{x}}{a}, y = \frac{\bar{y}}{a}, u = \frac{\bar{u}a}{\nu_o}, t = \frac{\nu_o \bar{t}}{a^2}, \theta = \frac{T-T_o}{T_1-T_o}, \phi = \frac{C-C_o}{C_1-C_o},$$
$$P = \frac{\mu_o^2 \bar{P}}{\rho a^2}, \mathrm{Re} = \frac{Va}{\nu_o}, A = -\frac{d\bar{P}}{dx}, A_1 = \gamma(T_1-T_o), M^2 = \frac{\sigma B_o^2 a^2}{\mu_o},$$
$$Gr = \frac{\beta_1 g a^3 (T_1-T_o)}{\nu_o}, Gc = \frac{\beta_2 g a^3 (C_1-C_o)}{\nu_o}, \mathrm{Pr} = \frac{\nu_o}{\alpha}, Sc = \frac{\nu_o}{D_B},$$
$$Nb = \frac{\tau D_B (C_1-C_o)}{\nu_o}, Nt = \frac{\tau D_T (T_1-T_o)}{T_o \nu_o}, Ec = \frac{V^2}{c_p a^2 (T_1-T_o)}. \quad \ldots (8)$$

Then we have non-dimensional PDEs:

$$\frac{\partial u}{\partial t} + \mathrm{Re}\frac{\partial u}{\partial y} = A - A_1 e^{A_1\theta}\frac{\partial \theta}{\partial y}\frac{\partial u}{\partial y} + e^{A_1\theta}\frac{\partial^2 u}{\partial y^2} - M^2 u + Gr\theta + Gc\phi, \quad \ldots (9)$$

$$\mathrm{Pr}\frac{\partial \theta}{\partial t} + \mathrm{Pr}\,\mathrm{Re}\frac{\partial \theta}{\partial y} = \frac{\partial^2 \theta}{\partial y^2} + \mathrm{Pr}\,Nb\frac{\partial \phi}{\partial y}\frac{\partial \theta}{\partial y} + \mathrm{Pr}\,Nt\left(\frac{\partial \theta}{\partial y}\right)^2 + \mathrm{Pr}\,Ec\left(\frac{\partial u}{\partial y}\right)^2 e^{-A_1\theta} + \mathrm{Pr}\,M^2 Ec\cdot u^2, \quad \ldots (10)$$

$$Sc\frac{\partial \phi}{\partial t} + \mathrm{Re}\,Sc\frac{\partial \phi}{\partial y} = \frac{\partial^2 \phi}{\partial y^2} + \frac{Nt}{Nb}\frac{\partial^2 \theta}{\partial y^2}, \quad \ldots (11)$$

with initial and boundary conditions

$$u(y,0) = 0, \theta(y,0) = 0, \phi(y,0) = 0, \quad \ldots (12)$$

$$u(0,t) = 0, \theta(0,t) = 0, Nb\frac{\partial \phi}{\partial y}(0,t) = -Nt\frac{\partial \theta}{\partial y}(0,t),$$
$$u(1,t) = 0, \theta(1,t) = 1, \phi(1,t) = 1, \quad \ldots (13)$$

where Re is the Reynold suction/injection parameter, A is the pressure gradient parameter, A_1 is the viscosity variation parameter, M is magnetic field parameter, Gr is the thermal Grashof number, Gc is the solutal Grashof number, Pr is the Prandtl number, Nb is the Brownian motion parameter, Nt is the thermophoretic parameter, Ec is the Eckert number and Sc is the Schmidt number.

The important physical quantities of interest in the study of the problem are the local skin friction Cf, the local Nusselt number Nu, and the local Sherwood number Sh, where

$$\phi(y_i,t),\ Cf = \frac{\tau_w}{\rho V^2}, Nu = \frac{aq_w}{k(T_1-T_o)}, Sh = \frac{aq_m}{D_B(C_1-C_o)}. \quad \ldots (14)$$

But $\tau_w = \mu\left.\frac{\partial \bar{u}}{\partial \bar{y}}\right|_{\bar{y}=0,a}, q_w = -k\left.\frac{\partial T}{\partial \bar{y}}\right|_{\bar{y}=0,a}, q_m = -D_B\left.\frac{\partial C}{\partial \bar{y}}\right|_{\bar{y}=0,a}$.

The non-dimensional forms of equation (14) are:

$$\mathrm{Re}^2 Cf = e^{-A_1\theta}\cdot\left.\frac{\partial u}{\partial y}\right|_{y=0,1}, Nu = -\left.\frac{\partial \theta}{\partial y}\right|_{y=0,1}, Sh = -\left.\frac{\partial \phi}{\partial y}\right|_{y=0,1}. \quad \ldots (15)$$

3 Numerical Methods

The model nonlinear Eqs. 9-13 are a system of initial boundary value problems (IBVPs) and their solutions are obtained by using a semi-discretization via finite difference scheme with *Runge-Kutta Fehlberg* integration technique. Spatial interval [0,1] is subdivided into $N+1$ equal subintervals. The nodal spacing and nodal points are defined respectively as $\Delta y = \frac{1}{N+1}$ and $y_i = i\Delta y$, for $i = 1,2,...,N$ where N is the number of interior nodal points in [0,1]. The first and second spatial derivatives are replaced by a finite difference approximation of order $(\Delta y)^2$ accuracy. Let u_i, θ_i, and ϕ_i, represent $u(y_i,t)$, $\theta(y_i,t)$, and $\phi(y_i,t)$, respectively. Then the semi-discretization scheme with centered finite difference

method for Eqs. 9-13 reduced to:

$$\frac{du_i}{dt}+\mathrm{Re}\left(\frac{u_{i+1}-u_{i-1}}{2\Delta y}\right)=A-A_1e^{-A_1\theta_i}\left(\frac{\theta_{i+1}-\theta_{i-1}}{2\Delta y}\right)\left(\frac{u_{i+1}-u_{i-1}}{2\Delta y}\right)$$
$$+e^{-A_1\theta_i}\left(\frac{u_{i+1}-2u_i+u_{i-1}}{(\Delta y)^2}\right)-M^2u_i+Gr\theta_i+Gc\phi_i \quad \ldots (16)$$

$$\mathrm{Pr}\frac{d\theta_i}{dt}+\mathrm{Pr}\,\mathrm{Re}\left(\frac{\theta_{i+1}-\theta_{i-1}}{2\Delta y}\right)=\left(\frac{\theta_{i+1}-2\theta_i+\theta_{i-1}}{(\Delta y)^2}\right)$$
$$+\mathrm{Pr}\,Nb\left(\frac{\phi_{i+1}-\phi_{i-1}}{2\Delta y}\right)\left(\frac{\theta_{i+1}-\theta_{i-1}}{2\Delta y}\right)+\mathrm{Pr}\,Nt\left(\frac{\theta_{i+1}-\theta_{i-1}}{2\Delta y}\right)^2 \quad \ldots (17)$$
$$+\mathrm{Pr}\,Ec\left(\frac{u_{i+1}-u_{i-1}}{2\Delta y}\right)^2e^{-A_1\theta_i}+\mathrm{Pr}\,EcM^2u_i^2,$$

$$Sc\frac{d\phi_i}{dt}+\mathrm{Re}\,Sc\left(\frac{\phi_{i+1}-\phi_{i-1}}{2\Delta y}\right)=\left(\frac{\phi_{i+1}-2\phi_i+\phi_{i-1}}{(\Delta y)^2}\right)$$
$$+\frac{Nt}{Nb}\left(\frac{\theta_{i+1}-2\theta_i+\theta_{i-1}}{(\Delta y)^2}\right), \quad \ldots (18)$$

with initial conditions

$$u_i(0)=0,\theta_i(0)=0,\phi_i(0)=0,\ \ 1\le i\le N. \quad \ldots (19)$$

The boundary conditions at $y=0,1$ are transformed as follows:

$$u_o(t)=0,\theta_o(t)=0,Nb\frac{d\phi_o(t)}{dy}=0\left(\frac{\phi_1(t)-\phi_o(t)}{\Delta y}=0\right), \quad \ldots (20)$$
$$u_{N+1}(t)=0,\theta_{N+1}(t)=1,\phi_{N+1}(t)=1.$$

Eqs. 16-20 is a system of first order nonlinear ordinary differential equations with known initial conditions and its solution can be obtained successively by *Runge-Kutta Fehlberg* integration techniques[43].

4 Results and Discussion

All the effects of magnetic field, temperature dependent viscosity, Brownian motion, thermophoresis, and mixed convective heat transfer on unsteady nanofluid flow in a microchannel with permeable walls are analyzed. The semi-discretization method via centered finite difference scheme with *Runge-Kutta Fehlberg* integration technique is used to solve numerically the governing nonlinear IBVPs. Numerical solution for the velocity profiles, temperature profiles, nanoparticles concentration profiles, skin friction, Nusselt number and Sherwood number are carried out by assigning some specific values to various governing parameters of the nanofluid flow system. The results are shown in Figs. 2-24.

4.1 Transient velocity, temperature and concentration profile

Figures 2-5 depict the transient effects on the velocity, temperature and concentration profiles for fixed values of governing parameters. The fluid flow velocity increases from zero value in time and space at both left and right fixed plates to its maximum value within the microchannel as seen in Fig. 2(a). Figure 2(b) shows the fluid temperature augments from its zero value at the left plate to its maximum value at the right plate. The nanoparticles concentration of the fluid reduced from its maximum value in time and space near the left plate ($y=0$) to its constant value at the right plate

($y=1$) in Fig. 2(c). Meanwhile, an increase time, rises the fluid velocity to its maximum value around the hub of the channel until a steady state is attained as illustrated in Figs. 3(a-b). Moreover, the velocity reaches steady state quickly

when the fluid is injected in to the channel ($\mathrm{Re}<0$) compared with suction ($\mathrm{Re}>0$). From

Figs. 4(a- b), it is observed that fluid temperature has noticeable value at the right plate ($y=1$) within short period of time. As time increases, temperature of the fluid rises until the steady state is attained. It can be noticed from Figs. 5(a-b) that nanoparticles concentration increases in the whole channel region for $t\le 0.5$ and decreases for $t>0.5$ until a steady state constant concentration value is attained at the right plate ($y=1$). Moreover, there is a dynamic fluctuation of concentration value near $y=1$ for $0.1\le t\le 0.5$

4.2 The steady state velocity profiles

The effects of governing parameter variation on steady state velocity profiles are illustrated in Figs. 6-9. Figures 6(a-b) displays the influence of suction/injection parameter Re on nanofluid velocity. It is observed in Fig. 6(a) that as suction parameter $\mathrm{Re}>0$ increases, the velocity of the nanofluid decreased in the channel at the left wall and centerline before a reversal flow phenomenon near the right permeable wall happens. This is expound as increasing suction $\mathrm{Re}>0$ at the right hot wall imply

that more nanofluid which are heated get kinetic

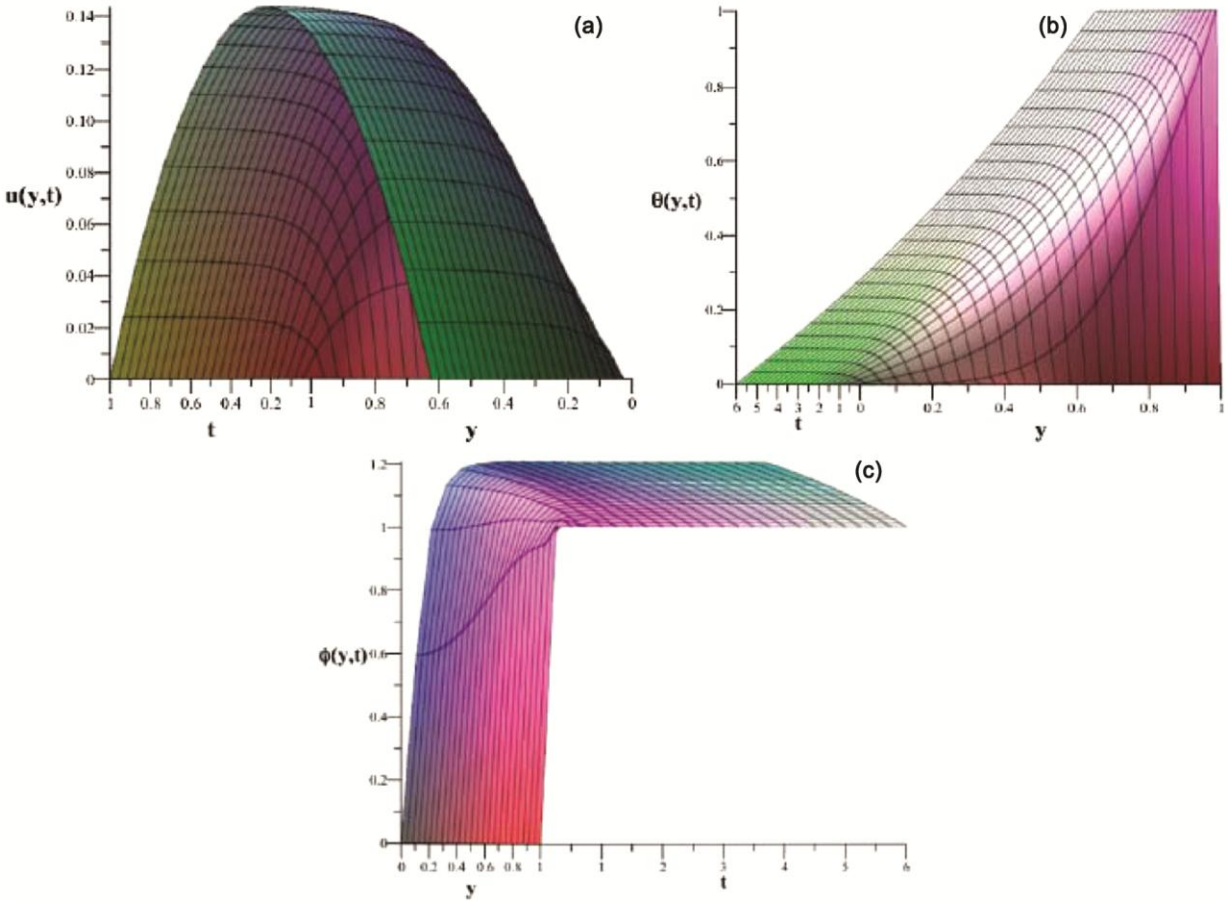

Fig. 2 — Fluid velocity, temperature and concentration across the channel with increasing time t (Re = M = Gc = Gr = Nt = Ec = A_1 = 0.1, Nb = 0.5, Sc = 0.6, Pr = 6.2, A = 1).

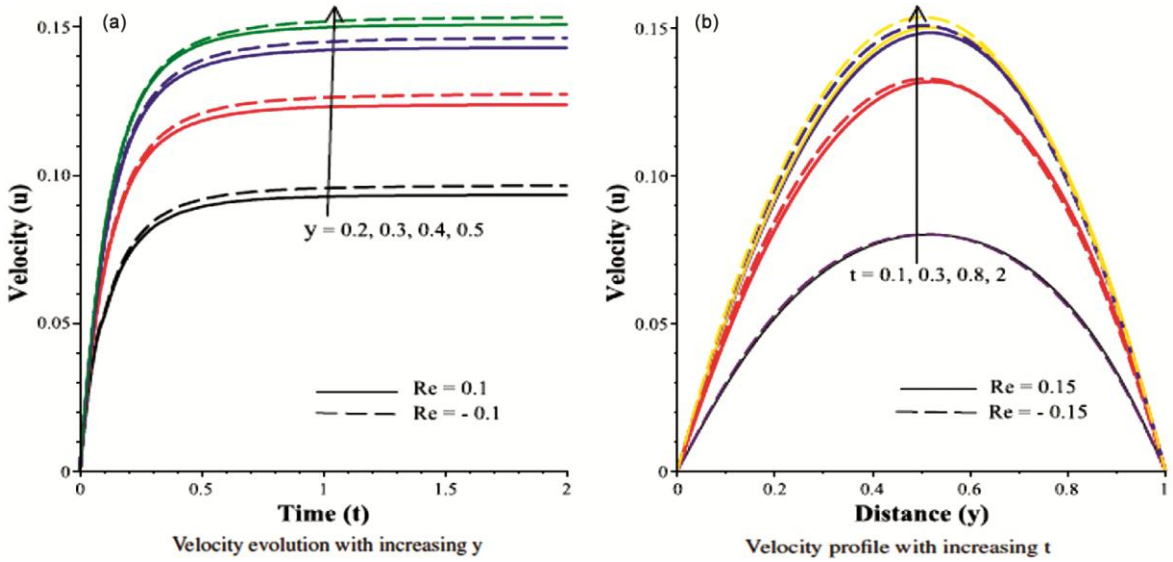

Fig. 3 — Fluid velocity across the channel with increasing time (M = Gc = Gr = Nt = Ec = A_1 = 0.1, Nb = 0.5, Sc = 0.6, Pr = 6.2, A = 1).

energy at the right wall. This leads to increase the velocity of the nanofluid at right wall. Again, as injection parameter $\mathrm{Re} < 0$ increases, the velocity of the fluid decreased at the left wall and centerline of the channel followed by increase fluid velocity near the right wall of the channel. This is due to the injection of cold nanofluid to the flow channel through the left permeable wall which allow to decrease the velocity of the nanofluid near left permeable wall and the centerline. Figure 6(b) shows nanofluid velocity for different values of variable viscosity parameter A_1 in the presence of suction and injection. It can be seen that as A_1 increases, the nanofluid flow velocity increases in the microchannel in simultaneous presence of suction and injection. This is because increasing A_1 will make the viscosity of the fluid gets decreased. Further, the effect of A_1 on the flow velocity of nanofluid in the microchannel becomes more magnified in the presence of injection $\mathrm{Re} < 0$ than suction $\mathrm{Re} > 0$ except near the right wall.

In Figs. 7-8, it is observed that the rise in nanofluid velocity with an increase in pressure gradient, Eckert number, solutal Grashof number and thermal Grashof number parameter. As Gc and Gr increase, the buoyancy effect increases due to concentration and temperature gradient, which lead to an increase in velocity profile. Similar effect of increasing velocity results from increasing viscous dissipation within the flow system as Ec increases.

In Figs. 9(a-b), the effects of magnetic field and magnetic field with variable viscosity parameters on

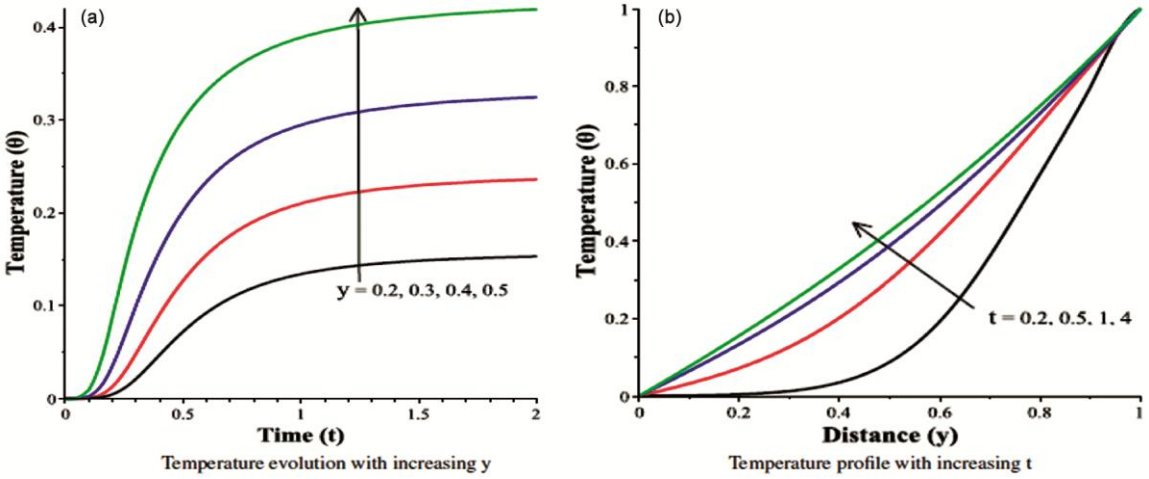

Fig. 4 — Fluid temperature across the channel with increasing time ($\mathrm{Re} = M = Gc = Gr = Nt = Ec = A_1 = 0.1, Nb = 0.5, Sc = 0.6, \mathrm{Pr} = 6.2, A = 1$).

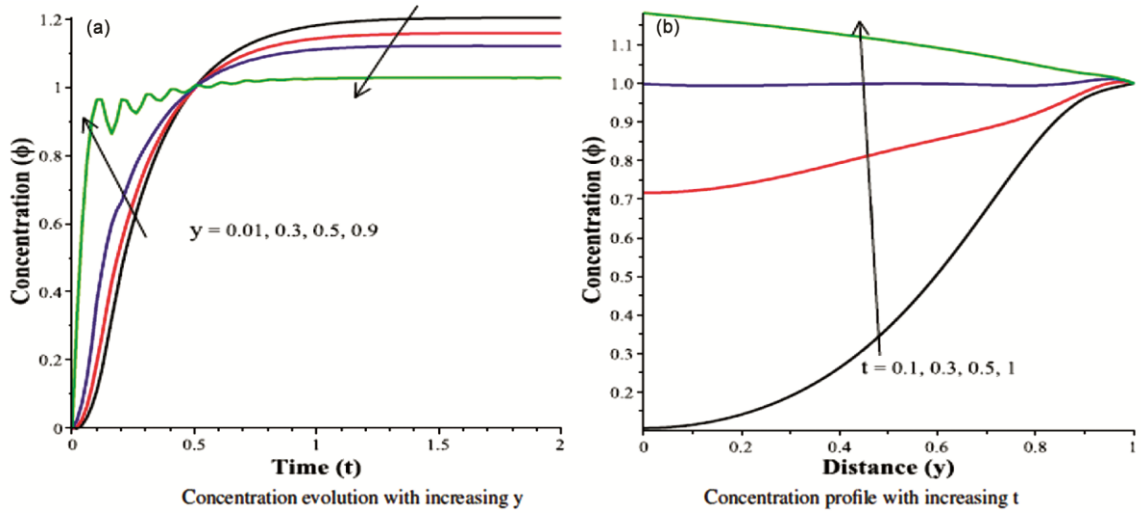

Fig. 5 — Fluid concentration across the channel with increasing time ($\mathrm{Re} = M = Gc = Gr = Nt = Ec = A_1 = 0.1, Nb = 0.5, Sc = 0.6, \mathrm{Pr} = 6.2, A = 1$).

velocity profile are highlighted. From Figs. 9(a-b), it is demonstrated that an increase in magnetic field parameter M has a retarding effect on the velocity of nanofluid across the microchannel, but strong retarding effect of velocity is observed on the centerline of the channel. It is obviously seen that the transverse magnetic field reduces the transport phenomena. This is due to the fact that change of magnetic field M gives rise to the change of Lorentz force, because of the presence of magnetic field, and the Lorentz force produces resistance to the transport phenomena. This is in agreement with the physics. In addition, for a fixed magnetic field parameter M, as viscosity variation parameter A_1 increases there is an increase in the nanofluid velocity as shown in Fig. 9(b).

4.3 The Steady State temperature profiles

Figure (10-12) explicate the temperature profile variation of nanofluid for different values of physical parameters. Figure 10(a) depicts the temperature profile with increasing suction/injection parameter Re. It is observed that the nanofluid temperature dwindled with increasing both suction and injection parameter. The dependence of temperature profile on Prandtl number is presented in Fig. 10(b). Prandtl number Pr is inversely related to thermal conductivity of the fluid. From the figure it is easily seen that the nanofluid temperature profile decreased with an augmentation in Prandtl number. The impact of nanoparticle parameters Nb, Nt on nanoparticles temperature profile is shown in Figs. 11(a-b). Increasing Nb enhances the Brownian motion force. There is a random movement of nanoparticles along

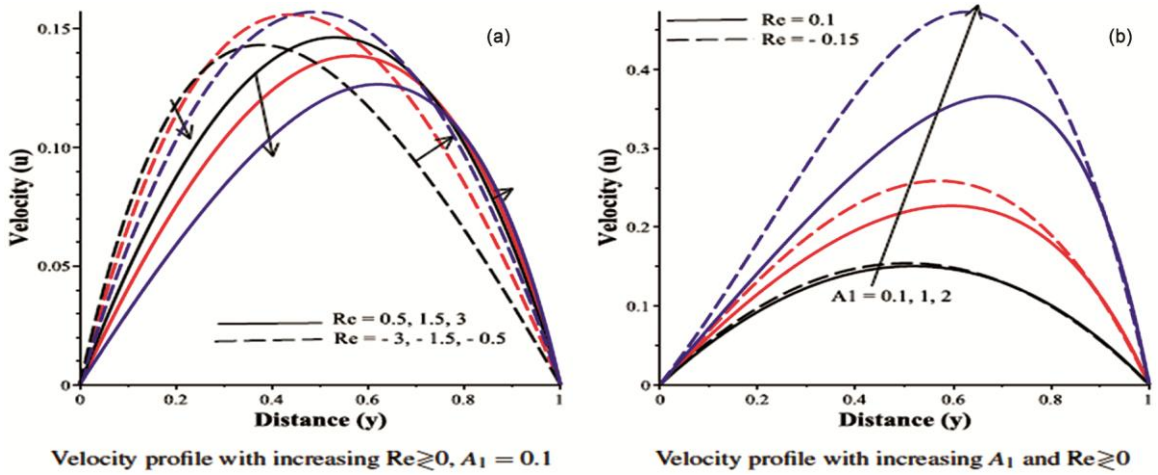

Fig. 6 — Steady state velocity profiles with increasing Re, A_1 ($M = Gc = Gr = Nt = Ec = 0.1, Nb = 0.5, Sc = 0.6, \Pr = 6.2, A = 1$).

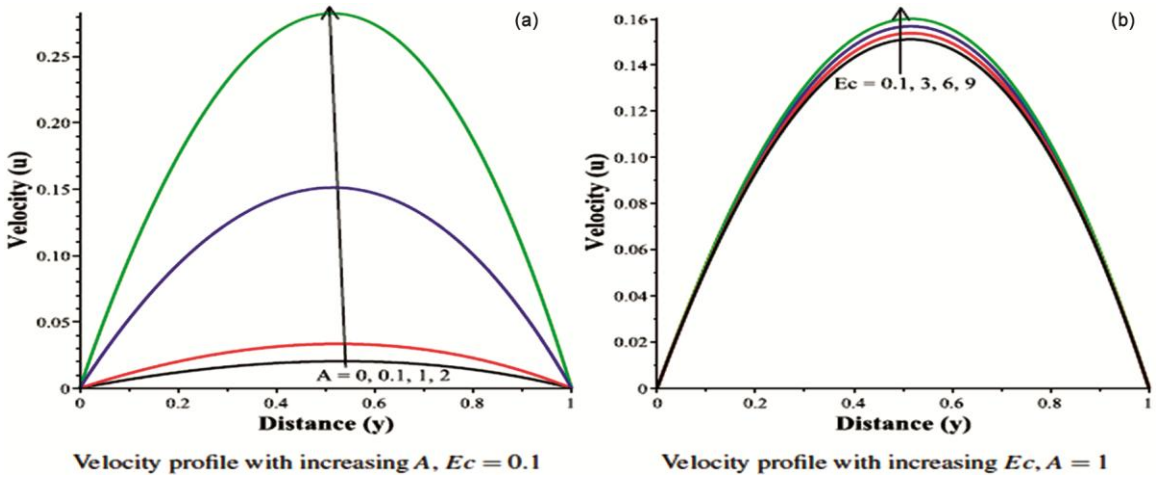

Fig. 7 — Steady state velocity profiles with increasing A, Ec (Re = $M = Gc = Gr = Nt = A_1 = 0.1, Nb = 0.5, Sc = 0.6, \Pr = 6.2$).

the concentration gradient due to Brownian motion force. This random movement of nanoparticles increases the kinetic energy of the particles in the fluid which raises the heat transfer rate. Therefore, the temperature of nanofluid decreased across the channel as shown in Fig. 11(a). An increase in Nt augments the thermophoretic force. The thermophoretic force pushes the nanoparticles from the heated wall toward the core region - in the direction of heat transfer- which leads to raise the nanoparticle concentration in the flow field. The rise of nanoparticle in the flow field will increase the heat transfer rate which in turn reduces the temperature profile of the nanofluid as seen in Fig. 11(b). Figure 12(a) is sketched to highlight the property of temperature profile with Eckert number Ec. From the definition of Eckert number Ec, a positive Ec directly related to heating (heat is being supplied across the wall in to the fluid). There is a significant rise in the temperature of the nanofluid with an increase in Ec. This rise in nanofluid temperature is a reason for generation of internal heat due to viscous dissipation in the flow field. It is noticed that nanofluid temperature profile is increasing across the channel with an augment in variable viscosity parameter A_1 as seen in Fig. 12(b).

4.4 The Steady State Concentration Profile

The nanoparticles concentration profiles under the influence of nanofluids parameters (Nt, Nb), pressure gradient and Schmidt number (A, Sc), buoyancy parameter (Gc, Gr), and Reynold and Eckert numbers (Re, Ec) are shown in Figs. 13(a-b) & 14(a-b), respectively. An increase in thermophoretic parameter Nt amplifies the nanoparticle concentration, whereas the Brownian motion parameter Nb decreases the nanoparticle concentration across the microchannel as shown in Fig. 13(a). Moreover, the highest and

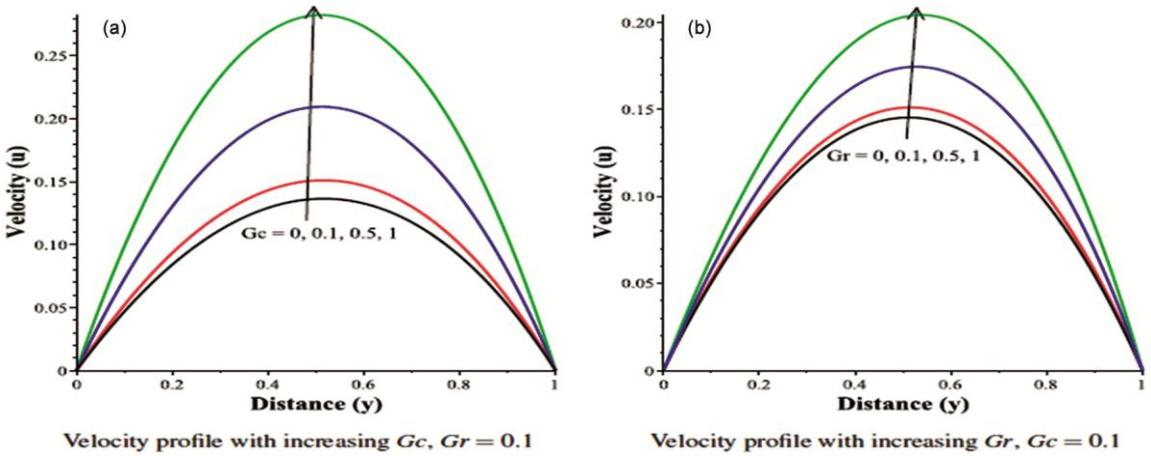

Fig. 8 — Steady state velocity profiles with increasing Gc, Gr $(\mathrm{Re} = M = Nt = Ec = A_1 = 0.1, Nb = 0.5, Sc = 0.6, \mathrm{Pr} = 6.2, A = 1)$.

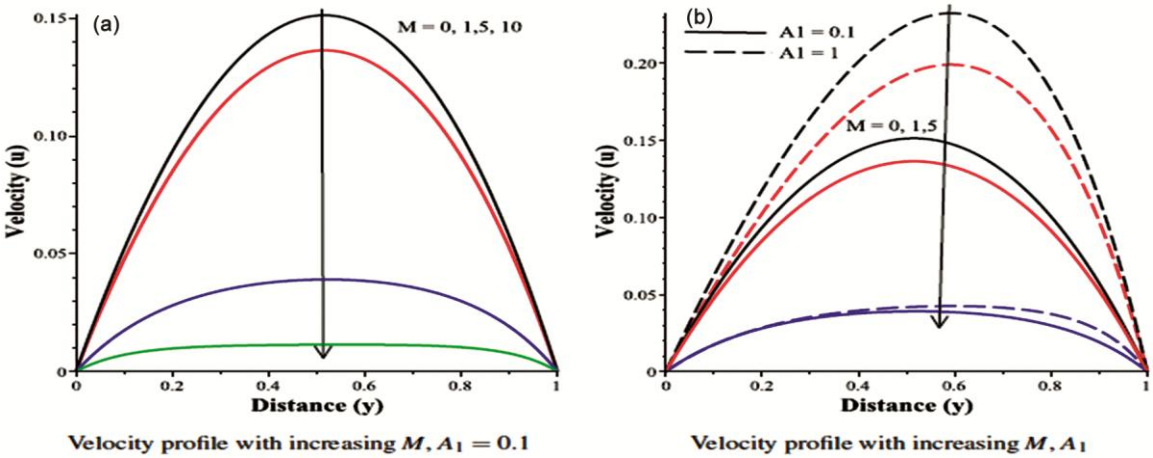

Fig. 9 — Steady state velocity profiles with increasing M, A_1 $(\mathrm{Re} = Gc = Gr = Nt = Ec = 0.1, Nb = 0.5, Sc = 0.6, \mathrm{Pr} = 6.2, A = 1)$.

smallest nanoparticle concentration is attained at $y=0$ and $y=1$ respectively for arbitrary variation of nanofluids parameters. The Schmidt number Sc describes the nanofluid flows where both momentum and mass diffusion convection processes occur simultaneously. When $Sc=1$, the momentum and mass diffusivities are equal and the nanoparticles concentration is obtained to be higher across the microchannel in the absence of pressure gradient as shown in figure 13(b). Also, an increase in pressure gradient reduces the nanoparticle concentration and a reverse trend happens with an increase in Schmidt number. Increasing both solutal and thermal Grashof number reduces the nanoparticles concentration across the microchannel as shown in Fig. 14(a). It is also seen that the highest nanoparticles concentration is found in the absence of both solutal and thermal Grashof numbers. As Eckert number increases, the nanoparticles concentration decreased in the microchannel in the existence of both suction and injection as shown in Fig. 14(b). Further, nanofluids particle concentration is found to be much concentrated across the microchannel in the presence of suction than injection.

4.5 Skin friction, Nusselt number and sherwood number

In section 4.1 above, it has been shown that velocity, temperature, and concentration attained their steady state within short interval of time (respectively when $t=1.5, t=2$ and $t=1$. Since skin friction Cf, Nusselt number Nu and Sherwood number Sh respectively depend on change in velocity, temperature, and concentration that are steady for

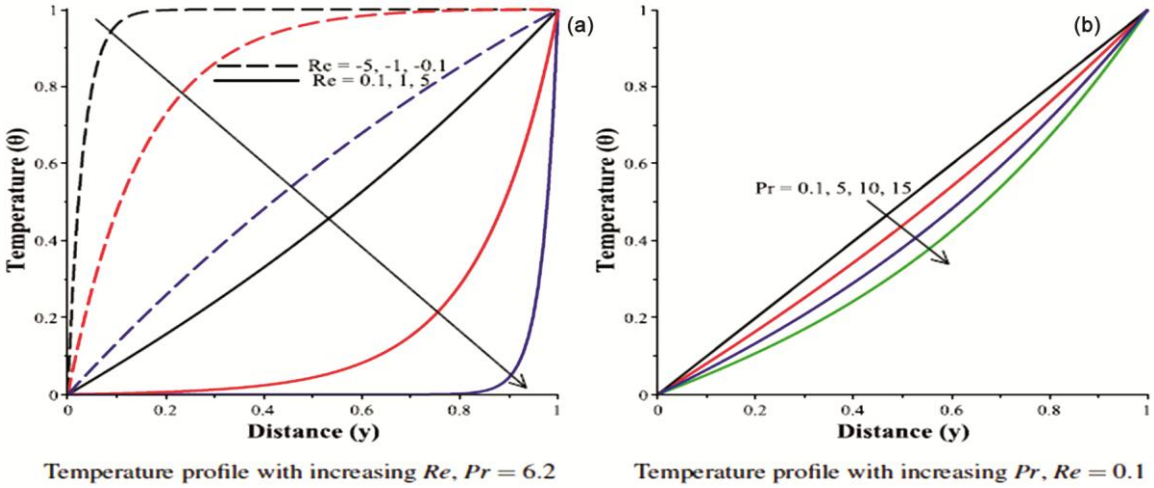

Fig. 10 — Steady state temperature profiles with increasing Re, Pr ($M=Gc=Gr=Nt=Ec=A_1=0.1, Nb=0.5, Sc=0.6, A=1$).

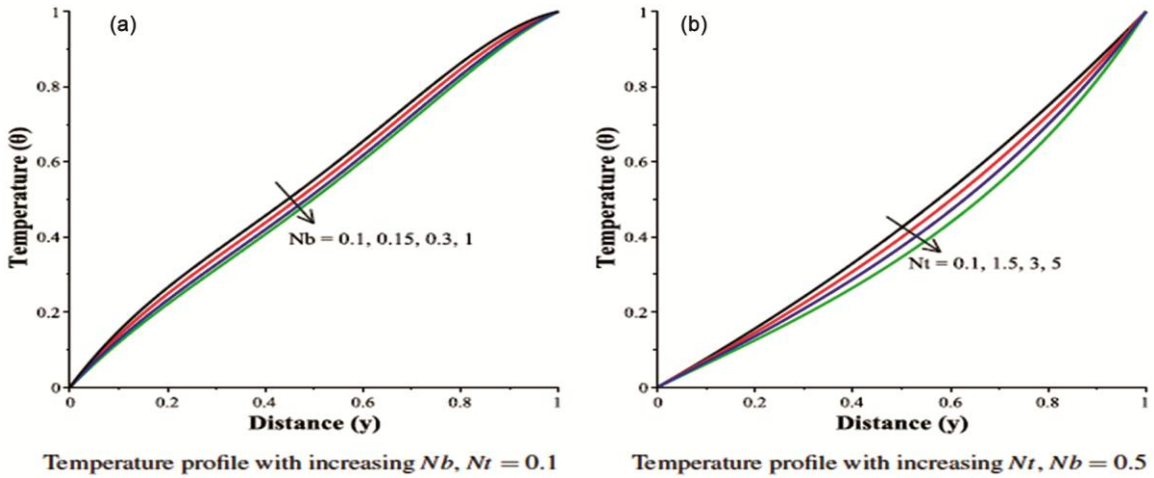

Fig. 11 — Steady state temperature profiles with increasing Nb, Nt ($\mathrm{Re}=M=Gc=Gr=Ec=A_1=0.1, Sc=0.6, \mathrm{Pr}=6.2, A=1$).

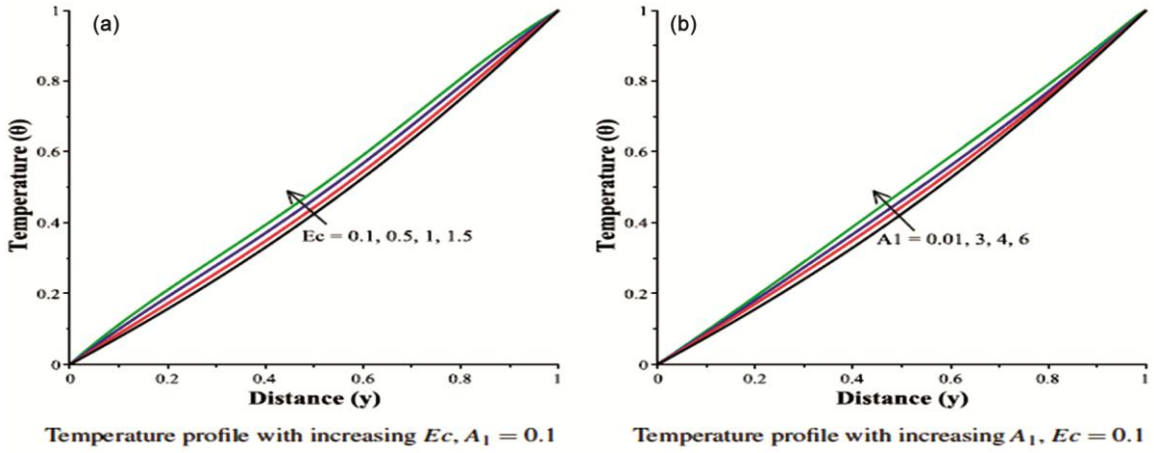

Fig. 12 — Steady state temperature profiles with increasing Ec, A_1 ($\mathrm{Re} = M = Gc = Gr = Nt = 0.1, Nb = 0.5, Sc = 0.6, \mathrm{Pr} = 6.2, A = 1$).

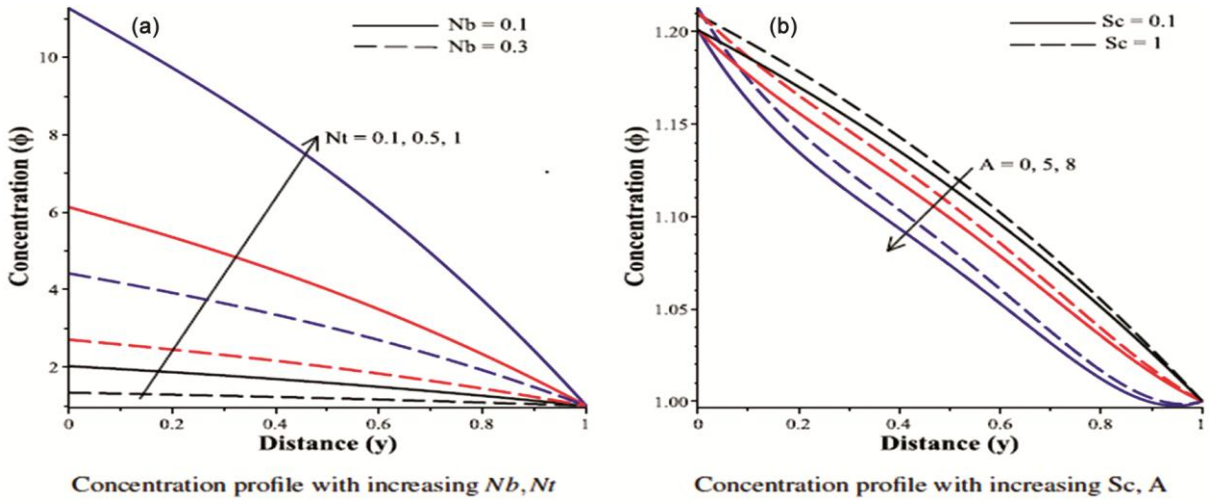

Fig. 13 — Steady state concentration profiles with increasing Nb, Nt ($\mathrm{Re} = M = Gc = Gr = Ec = A_1 = 0.1, \mathrm{Pr} = 6.2$).

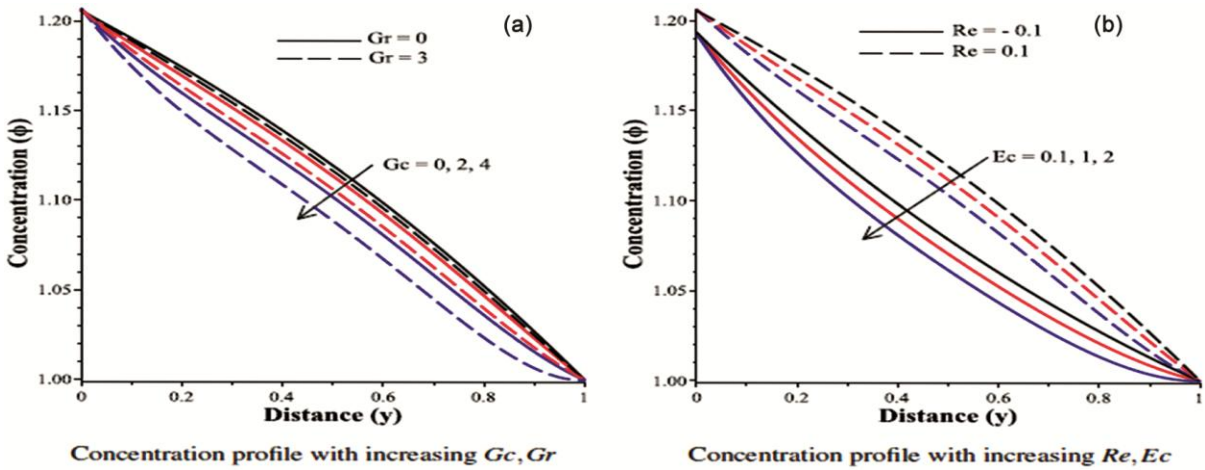

Fig. 14 — Steady state concentration profiles with increasing Gr, Gc, Re, Ec ($M = Nt = A_1 = 0.1, Nb = 0.5, Sc = 0.6, \mathrm{Pr} = 6.2, A = 1$).

large time t, it is reasonable to consider these quantities of engineering interest under steady state condition for large time t. Figs. 15-24 show the local skin friction, the local Nusselt number, and the local Sherwood number with variation in the numerical values of thermo-physical parameters embedded in the problem. The local skin friction numerical values are displayed graphically in Figs. 15-18. Figures 15-16 depict the effect of both suction $(\mathrm{Re}>0)$ and injection $(\mathrm{Re}<0)$, respectively, with viscosity variation parameter A_1 on skin friction at the microchannel parallel vertical walls. It can be seen from these figures that the skin friction lighten with increase of suction and escalates with an increase in magnitude of injection parameter at both microchannel plates $y=0$ and $y=1$. It is also found that an increase in viscosity variation parameter result in a decrease and an increase on local skin friction at the microchannel plate walls $y=0$ and $y=1$, respectively. The simultaneous effect of magnetic field and thermophoretic parameters on skin fiction at the microhannel walls $y=0$ and $y=1$ are revealed in Figs. 17(a-b), respectively. It can be concluded from Fig. 17(a) that an increase in magnetic field parameter diminishes the skin friction and it escalated with an increase in thermophoretic parameter at $y=0$. Figure

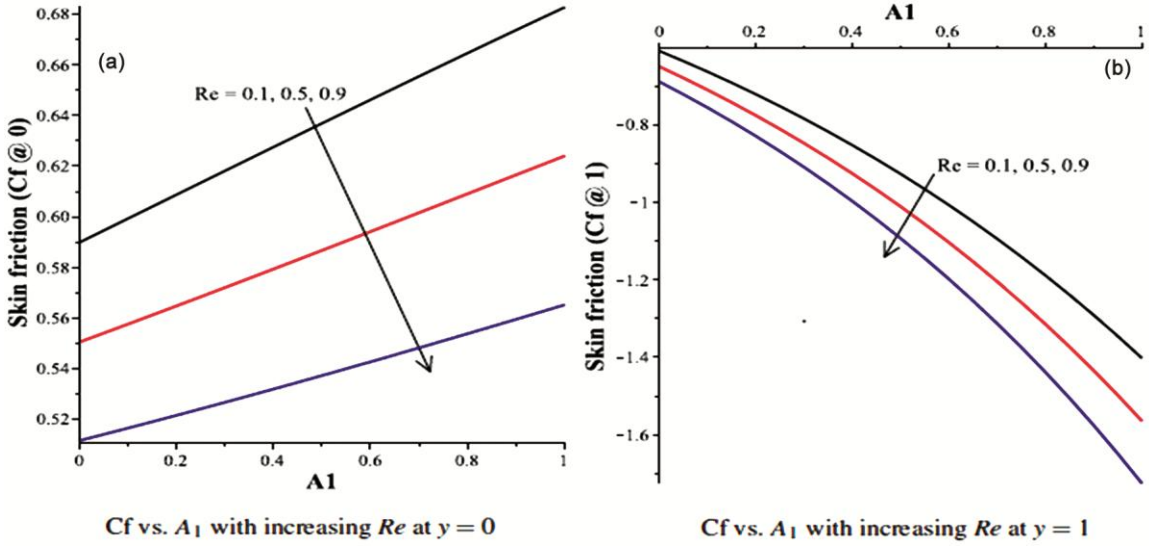

Fig. 15 — Skin friction versus A_1 with increasing Re $(M=Gc=Gr=Nt=Nb=Sc=Ec=0.1, \mathrm{Pr}=6.2, A=1)$.

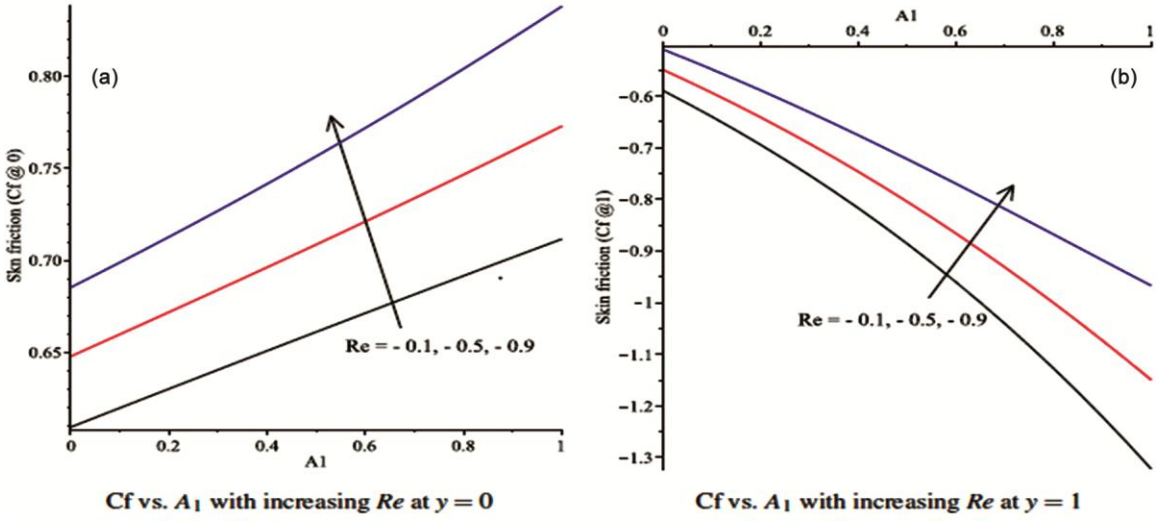

Fig. 16 — Skin friction versus A_1 with increasing Re $(M=Gc=Gr=Nt=Nb=Sc=Ec=0.1, \mathrm{Pr}=6.2, A=1)$.

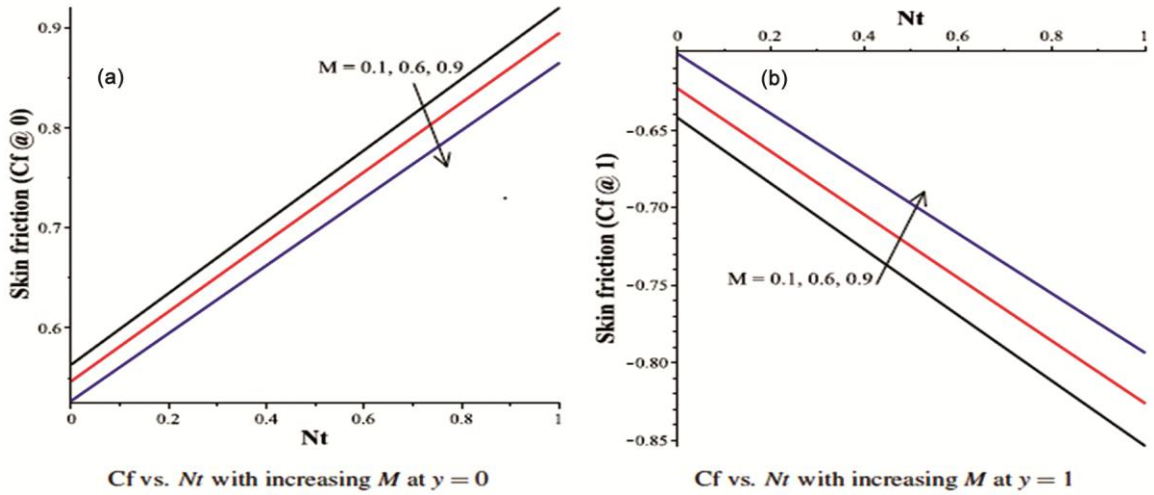

Fig. 17 — Skin friction versus Nt with increasing M (Re = $Gc = Gr = Nb = Sc = Ec = A_1 = 0.1$, Pr = 6.2, $A = 1$).

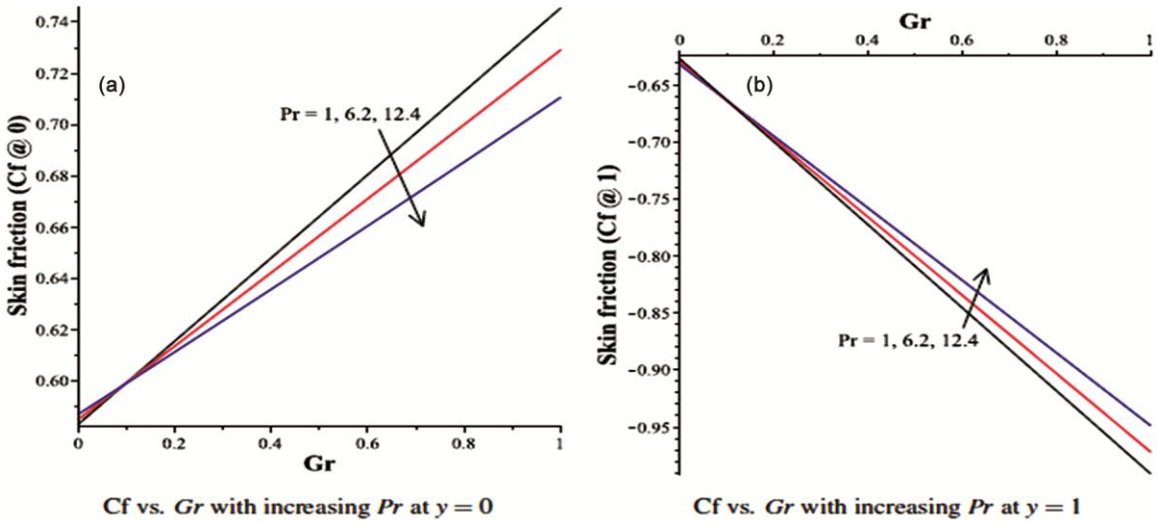

Fig. 18 — Skin friction versus Gr with increasing Pr (Re = $M = Gc = Nb = Sc = Ec = A_1 = 0.1$, $A = 1$).

17(b) shows the skin friction increases with magnetic field parameter and decreases with thermophoretic parameter at $y = 1$. Figure 18(a-b) illustrate the combined effect of Prandtl and thermal Grashof number on skin friction at the microchannel walls $y = 0$ and $y = 1$, respectively. From Fig. 18(a), it is evident in general that skin friction decreases with an increase in Prandtl number and increases with thermal Grashof number at $y = 0$, while a reverse trend is observed at $y = 1$ with an increase in Prandtl and thermal Grashof number as seen from Fig. 18(b). It is significant to note that at Grashof number $Gr = 0.1$ the skin friction at both plates' surfaces is not affected with increase the value of Prandtl number.

The change of local Nusselt number versus Eckert number for different values of viscosity variation parameter A_1 at $y = 0$ and $y = 1$ is illustrated in Figs. 19(a-b), respectively. It is observed that the local nusselt number at $y = 0$ decreases as both Eckert number and A_1 increase, while a reverse trend is observed at $y = 1$ with an increase in Eckert number and viscosity parameter simultaneously.

Figure 20 (a-b) show the change of local Nusselt number versus Schmidt number for different values of variable viscosity parameter at $y = 0$ and $y = 1$, respectively. From these figures we observed that as Schmidt number increases, the local Nusselt number augments at $y = 0$. Also, it decreases at $y = 1$ as

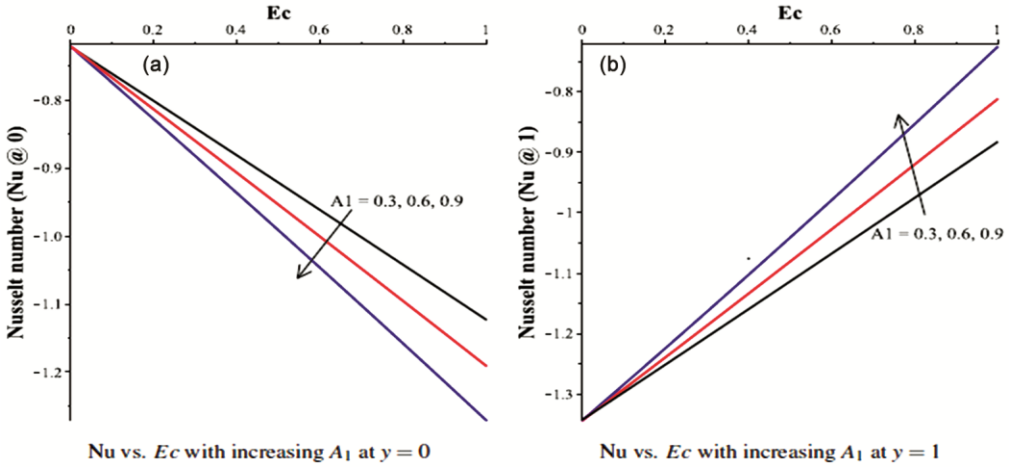

Fig. 19 — Nusselt number versus Ec with increasing A_1 (Re = $M = Gc = Gr = Nt = Nb = Sc = 0.1$, Pr = 6.2, $A = 1$).

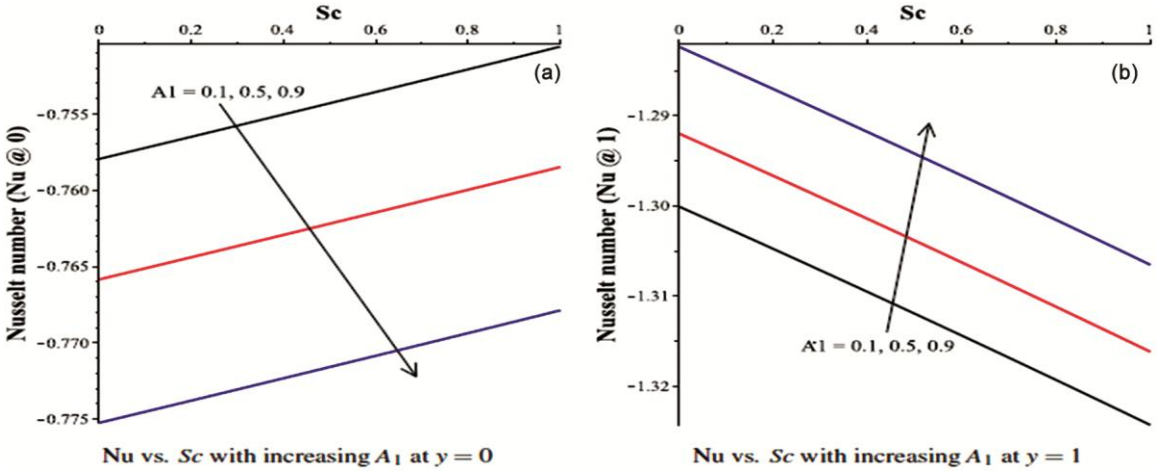

Fig. 20 — Nusselt number versus Sc with increasing A_1 (Re = $M = Gc = Gr = Nt = Nb = Ec = 0.1$, Pr = 6.2, $A = 1$).

Schmidt number increases. The variation of local Nusselt number with thermophoretic parameter Nt for various increaseing values of Brownian motionparameter Nb at plates $y = 0$ and $y = 1$ is shown in Fig. 21(a-b), respectively. In Fig. 21(a), as the thermophoretic parameter Nt magnified, the local Nusselt number at the plate $y = 0$ escalated at high Brownian motion parameter $Nb = 0.9$ and diminished at low Brownian motion parameter $Nb = 0.1$. Similarly, the local Nusselt number at the plate $y = 1$ decreased for large Brownian motion parameter $Nb = 0.9$ and increased for low Brownian motion parameter $Nb = 0.1$ as the thermophoretic parameter Nt increases.

Figure 22(a) entails that increasing local Sherwood number at $y = 0$ as both variable viscosity parameter A_1 and Eckert number Ec augments. An analogous trend of dwindled local Sherwood number is observed in Fig. 22(b) with increasing variable viscosity parameter A_1 and Eckert number Ec at $y = 1$. As Schmidt number Sc and magnetic field parameter M magnify, the local Sherwood number diminish at $y = 0$ as illustrated in Fig. 23(a). An overturn result on local Sherwood number at $y = 1$ is seen in Fig. 23(b) with increment in Schmidt number Sc and magnetic field parameter M. Figure 24(a-b) show the local Sherwood number versus thermophoretic parameter Nt for varying values of Brownian motion parameter Nb at $y = 0$ and $y = 1$, respectively. It is observed from these figures that local Sherwood number decreases with an increase in Brownian motion parameter Nb and increases with an increase

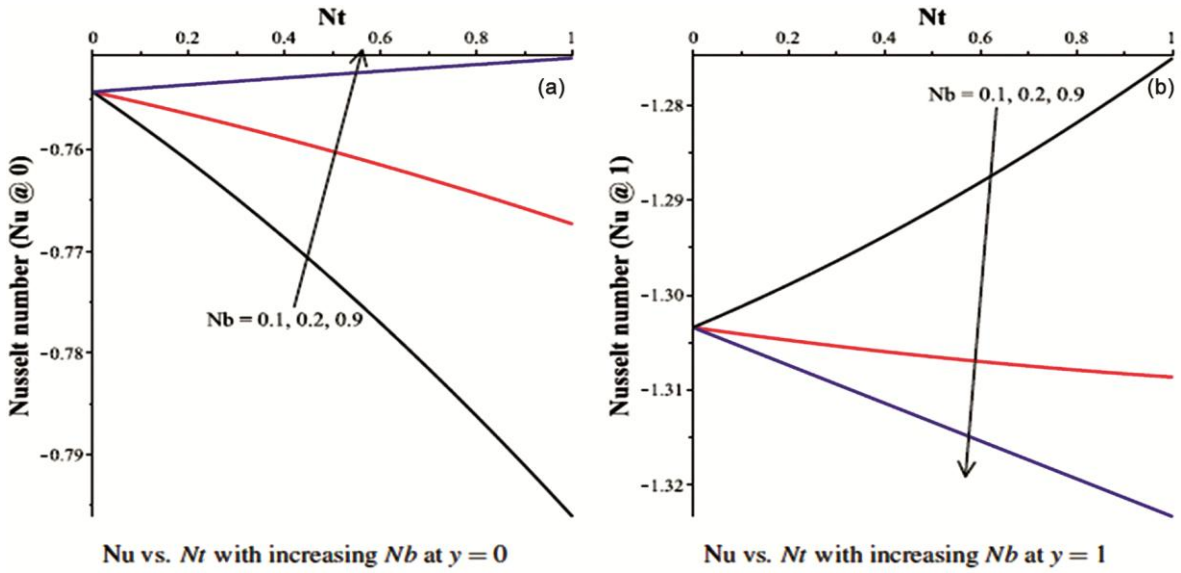

Fig. 21 — Nusselt number versus Nt with increasing Nb ($\mathrm{Re} = M = Gc = Gr = Sc = Ec = A_1 = 0.1, \mathrm{Pr} = 6.2, A = 1$).

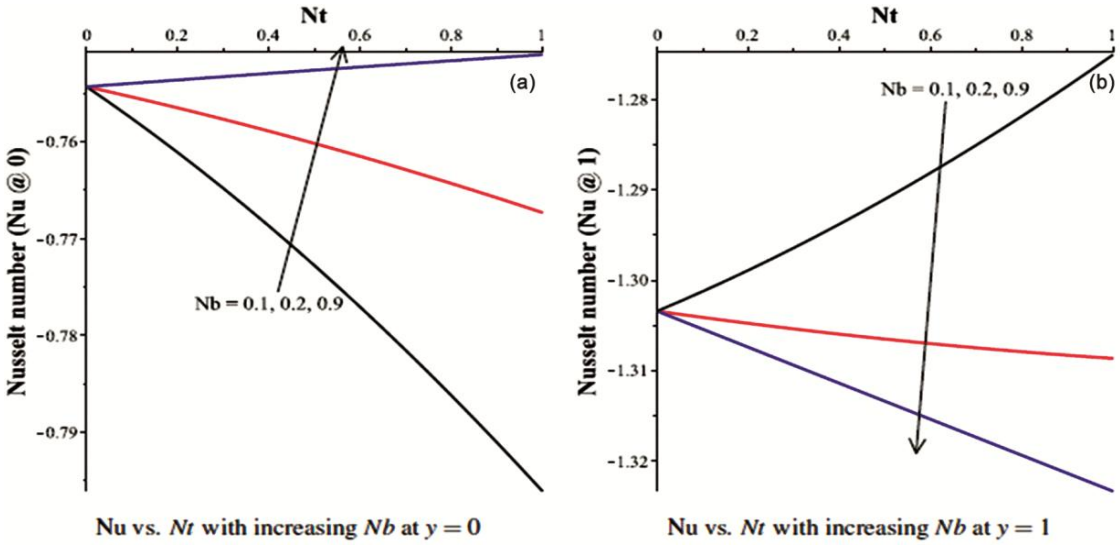

Fig. 22 — Sherwood number versus Ec with increasing A_1 ($\mathrm{Re} = M = Gc = Gr = Nt = Nb = Sc = 0.1, \mathrm{Pr} = 6.2, A = 1$).

in thermophoretic parameter Nt at both plates $y = 0$ and $y = 1$.

5. Summary and Conclusions

In this study, all the effects magnetic field, temperature dependent viscosity, Brownian motion, thermophoresis, and mixed convective heat transfer on unsteady nanofluid flow in a microchannel with permeable walls are analyzed. The governing nonlinear coupled PDEs were developed, nondimensionalized, and solved numerically by semi-discretization method via centered finite difference scheme with *Runge-Kutta Fehlberg* integration technique. Based on graphical results, the following pertinent conclusions are made:

- The nanofluid velocity reaches steady state quickly when the fluid is injected into the microchannel as compared with suction.
- A dynamic fluctuation of nanoparticle concentration is observed near the right plate $y = 1$ when the time t is between 0.1 and 0.5.
- The nanofluid velocity decreases at the left wall with an increase in suction/injection and an opposite phenomenon occurs at the right wall with suction/injection increment.

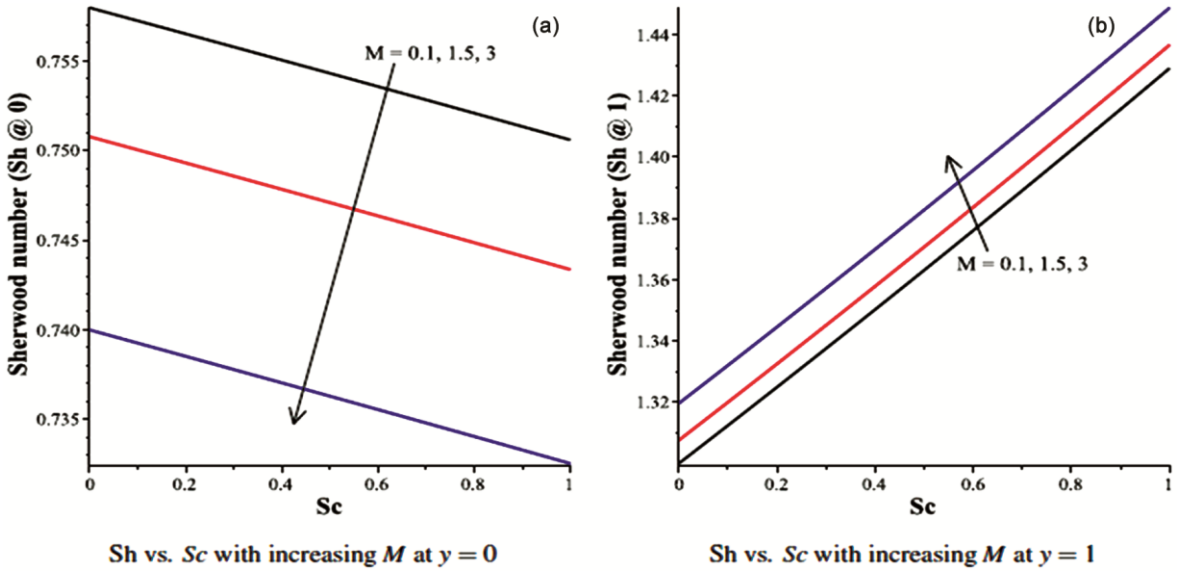

Fig. 23 — Sherwood number versus Sc with increasing M (Re = $Gc = Gr = Nt = Nb = Ec = A_1 = 0.1$, Pr = 6.2, $A = 1$).

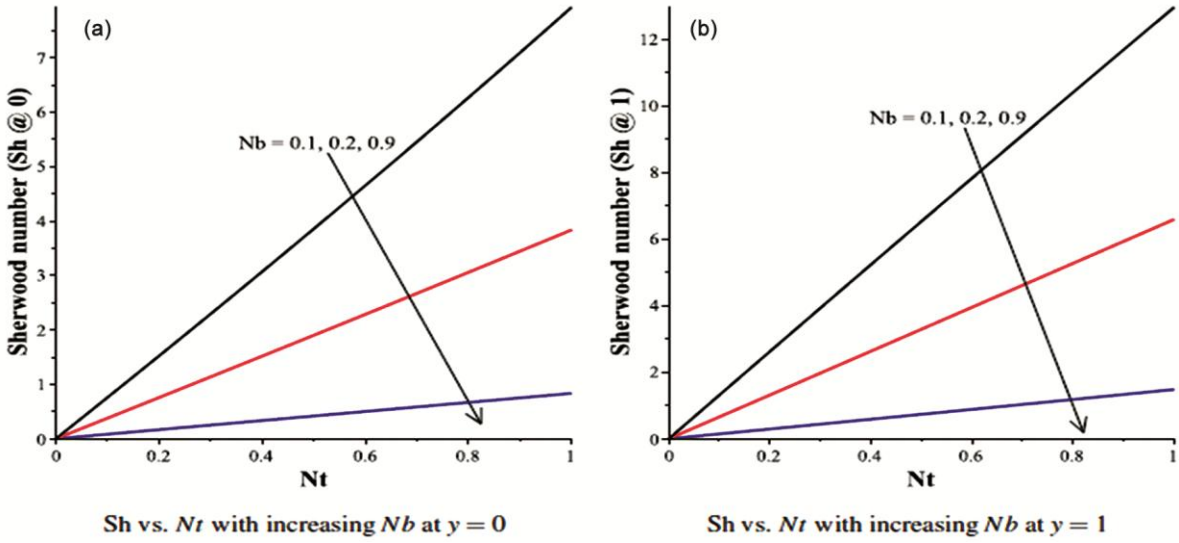

Fig. 24 — Sherwood number versus Nt with increasing Nb (Re = $M = Gc = Gr = Sc = Ec = A_1 = 0.1$, Pr = 6.2, $A = 1$).

- The nanofluid moves rapidly through the microchannel with increasing A_1, A, Ec, Gc and Gr, and moves slowly with increasing M. Moreover, a more retarding/ speeding up nanofluid velocity effect is seen at the centerline of the microchannel with a rise of influential parameters on velocity of the fluid.
- The nanofluid temperature increases across the microchannel with increasing Ec and A_1, and decreases with increasing Re, Pr, Nb and Nt.
- The nanoparticle concentration is increasing across the microchannel with increasing Nt and Sc, and reduced with increasing Nb, A, Gc, Gc, Gr and Ec. Further, nanoparticle concentration is much concentrated across the microchannel in the pressence of suction than injection.
- Increase in A_1, Nt and Gr enhance Cf while an increase in M and Pr lighten Cf at the wall $y = 0$. But Cf decreases with an increase A_1, Nt and Gr and increases with M and Pr at the wall $y = 1$.
- At the wall $y = 0$, Nu enhanced with rising Sc but diminished with increasing values of A_1 and Ec.

- At the wall $y=1$, Nu rises with amplifying values of A_1 and Ec and decreased with rising values of Sc.
- Increase in A_1, Ec, M and Sc enhance Sh at the wall $y=0$ and diminish Sh at the wall $y=1$.

References

1 Tuckerman D B & Pease R F W, *IEEE Electron Dev Lett*, 2 (1981) 126.
2 Sobhan C B & Garimella S V, *Microscale Thermophys Eng*, *5* (2001) 293.
3 Wu H Y & Cheng P, Int *J Heat Mass Trans*, 46 (2003) 2547.
4 Qu W & Mudawar I, *Int J Heat Mass Trans*, 45 (2002) 2549.
5 Wie W, Joshi Y & Patterson M K, *J Heat Trans*, 129 (2007) 1432.
6 Salari A, Navi M & Dalton C, *Biomicrofluidics*, 9 (2015) 014113.
7 Raisi A, Ghasemi B & Aminossadati S M, *Numer Heat Trans A: Appl*, 59 (2011) 114.
8 Salman B H, Mohammed H A, Munisamy K M & Kherbeet A S, *Renew Sustainable Energy Rev*, 28 (2013) 848.
9 Ibez G, Lpez A, Pantoja J & Moreira, J *Int J Heat Mass Trans*, 73 (2014) 201.
10 Malvandi A & Ganji D D, *Int J Therm Sci*, 84 (2014) 196.
11 Yang Y T, Wang Y H & Huang B Y, *Numer Heat Trans A: Appl*, 67 (2015) 571.
12 Avramenko A A, Tyrinov A I, Shevchuk I V, Dmitrenko N P, Kravchuk A V & Shevchuk V I, *Int J Heat Mass Trans*, 106 (2017) 1164.
13 Heydari M, Toghraie D & Akbari O A, *Therm Sci Eng Progress*, 2 (2017) 140.
14 Kandlikar S, Garimella S, Li D, Colin S & King M R, *Heat Trans Fluid Flow Minichannels Microchannels*, (USA), Elsevier, 2005.
15 Markal B, Aydin O & Avci M, *J Therm Sci Technol*, 38 (2018) 65.
16 Jha B K, Aina B & Ajiya A T, *Ain Shams Eng J,* 6 (2014) 289.
17 Jha B K, Aina B & Isa S, *Proc Mech E Part N: J Nanoeng Nanosyst*, (2015) 1.
18 Das S, Jana R N & Makinde O D, *Eng Sci Technol*, 30 (2015) 1.
19 Malvandi A & Ganji D D, *Physica E*, 66 (2015) 181.
20 Shashikumar N S, Prasannakumara B C, Gireesha B J & Makinde O D, *Diffusion Foundations*, 16 (2018) 120.
21 Aina B & Malgwi P B, *Nonlinear Eng*, 8 (2019) 755.
22 Kleinstreuer K, Li J & Koo J, *Int J Heat Mass Trans*, 51 (2008) 5590.
23 Bairwa D K, Upman K K & Kantak G, *Int J Eng Management Sci*, 2 (2015) 1.
24 Li J & Kleinstreuer C, *Int J Heat Fluid Flow*, 29 (2008) 1221.
25 Singh P K, Harikrishna P V, Sundararajan T & Das S K, *Experiment Therm Fluid Sci*, 42 (2012) 174.
26 Duangthongsuk W, Dalkilic A S & Wongwises S, *Current Nanosci*, 8 (2008) 317.
27 Bowersa J, Cao H, Qiao G, Li Q, Zhang G, Mura E & Ding Y, *Progress Natural Sci Mater Int*, 28 (2018) 225.
28 Trinavee K, Gogoi T K & Pandey M, *J Phys: Conf Ser*, 759 (2016) 1.
29 Malvandi A & Ganji D D, *J Appl Fluid Mech*, 9 (2016) 2277.
30 Belhadj A, Bouchenafa R & Saim R, *J Therm Eng*, 4 (2018) 2263.
31 Snoussi L, Ouerfelli N, Sharma K V, Vrinceanu N, Chamkha A J & Guizani A, *Phys Chem Liquids*, 56 (2018) 311.
32 Pordanjani A H, Raisi A & Ghasemi B, *Num Heat Trans A: Appl Int J Comput Methodol*, 1040 (2019) 1.
33 Nguyen Q, Bahrami D, Kalbasi R & Bach Q V, *Math Meth Appl Sci*, (2020) 1.
34 Jha B K, Aina B & Joseph S B, *J Process Mech Eng*, 228 (2013) 171.
35 Jha B K, Aina B & Ajiya A T, *Int J Energy Technol*, 7 (2015) 30.
36 Jha B K & Aina B, *J Nanofluids*, 5 (2016) 110.
37 Namburu P K, Kulkarni D P, Dandekar A & Das D K, *Micro Nano Lett*, 2 (2007) 67.
38 Khamis1 S, Makinde O D & Gyekye Y N, *Appl Comput Math*, 3 (2014) 75.
39 Prasad K V, Vaidya H & Vajravelu K, *J Appl Fluid Mech*, 8 (2015) 693.
40 Monaledi1 R L & Makinde O D, *Defect Diffusion Forum*, 387 (2018) 273.
41 Makinde O D, *Defect Diffusion Forum*, 387 (2018) 182.
42 Makinde O D & Franks O, *Cent Eur J Eng*, 4 (2014) 54.
43 Na T Y, *Computational methods in engineering boundary value problems*, (USA), ACADEMIC PRESS, 145 (1979).